Mucociliary transport velocity is decreased in nasal polyp mucosae despite vigorous ciliary beating

Thi Nga Nguyen
University of Occupational and Environmental Health Japan: Sangyo Ika Daigaku
Yuma Koga
University of Occupational and Environmental Health Japan: Sangyo Ika Daigaku
Tetsuro Wakasugi
University of Occupational and Environmental Health Japan: Sangyo Ika Daigaku
Takuro Kitamura
University of Occupational and Environmental Health Japan: Sangyo Ika Daigaku
Hideaki Suzuki (suzuhyde@med.uoeh-u.ac.jp)
University of Occupational and Environmental Health Japan: Sangyo Ika Daigaku
https://orcid.org/0000-0002-5262-1939

Research Article

Keywords: Mucociliary transport velocity, Ciliary beat frequency, Planar cell polarity proteins, Nasal polyp, Turbinate

Posted Date: December 16th, 2022

DOI: https://doi.org/10.21203/rs.3.rs-2333640/v1

Abstract

Background Mucociliary transport function in the airway mucosa is essential for maintaining a clean mucosal surface. This function is impaired in upper and lower airway diseases. Nasal polyps are a typical pathological feature of prolonged rhinosinusitis. Like the ordinary nasal mucosa, nasal polyps have a ciliated pseudostratified epithelium with vigorous ciliary beating. We herein measured ex vivo mucociliary transport velocity (MCTV) and ciliary beat frequency (CBF) and explored the expressions of planar cell polarity (PCP) proteins in nasal polyps in comparison with turbinate mucosae. Methods Inferior turbinates and nasal polyps were collected from patients with chronic rhinosinusitis during endoscopic sinonasal surgery. Ex vivo MCTV and CBF were measured using a high-speed digital imaging system. Expressions of PCP proteins were explored by fluorescence immunohistochemistry and quantitative RT-PCR. Results The MCTV of nasal polyps was significantly lower than that of the turbinates (7.43±2.01 vs. 14.56±2.09μm/s; P=0.0361), whereas CBF did not differ between the two tissues. The MCTV vector was pointed to the posteroinferior direction in all turbinates with an average inclination angle of 41.0 degrees. Immunohistochemical expressions of Dishevelled-1, Dishevelled-3, Frizzled3, Frizzled6, Prickle2 and Vangl2 were lower in the nasal polyps than in the turbinates. The expression levels of mRNAs for Dishevelled-1, Dishevelled-3 and Frizzled3 in the nasal polyps were also decreased in comparison with the turbinates. Conclusions These results indicate that ciliary transport in nasal polyps is impaired although vigorous ciliary beating is maintained, and that the impairment may be caused by a decrease in Dishevelled/Frizzled proteins and resultant PCP disarrangement.

Introduction

Mucociliary transport is an essential function in the airway mucosa to eliminate any foreign particles, allergens, and pathogens that may be adhering to the mucosal surface. The mucociliary transport function is mainly dependent on ciliary beating and the physical properties of the surface mucus. This function is known to be impaired in pathological conditions of the upper and lower airways, such as chronic sinusitis, allergic rhinitis, bronchial asthma, bronchiectasis, chronic obstructive pulmonary disease, and cystic fibrosis [1-4].

Nasal polyps are inflammatory outgrowths of the sinonasal mucosa that are typical pathological changes of prolonged allergic/nonallergic rhinosinusitis. Like the ordinary nasal mucosa, nasal polyps have ciliated pseudostratified epithelia [5]. Interestingly, our recent study showed that nasal polyp tissue exhibited vigorous ciliary beating and the baseline ciliary beat frequency (CBF) of this tissue was not decreased compared to that of the turbinate mucosae [6]. We conjectured that, although the CBF is maintained at the same level in nasal polyps as in the ordinary nasal mucosa, the temporal and/or spatial coordination of the ciliary movement may be impaired in the former, which would lead to a decline in the mucociliary clearance function of this tissue.

In the present study, we measured the *ex vivo* mucociliary transport velocity (MCTV) of nasal polyps in comparison with that of the inferior turbinate mucosae, and also explored the expressions of planar cell

polarity (PCP) proteins, which are responsible for coordinating cell polarization in epithelial tissues.

Materials And Methods

Patients and sample collection

A total of 30 chronic rhinosinusitis patients with hypertrophic rhinitis and/or nasal polyps were enrolled in this study. They consisted of 22 males and 8 females, aged 17-81 years, with an average age of 50.0 years. Total and/or specific serum IgE levels were positive in 23 patients (76.7%). Specific serum IgE levels were measured for house dust mites, Japanese cedar pollen, cypress pollen, orchard grass pollen, short ragweed pollen, timothy grass pollen and *Aspergillus*, which are major airborne allergens in Japan. Five patients had bronchial asthma.

The patients underwent endoscopic sinonasal surgery including turbinectomy and/or nasal polypectomy under general anesthesia. In turbinectomy, the inferior turbinate bone was resected together with the lateral mucosa of the turbinate. The collected inferior turbinates and nasal polyps were immediately soaked in O_2-saturated Hank's balanced salt solution (HBSS; 8000 (in mg/L) NaCl, 400 KCl, 350 $NaHCO_3$, 140 $CaCl_2$, 100 $MgCl_2 \cdot 6H_2O$, 100 $MgSO_4 \cdot 7H2O$, 60 KH_2PO_4, 47.8 Na_2HPO_4, and 1000 glucose) and thoroughly washed with HBSS to remove surface mucus. The lateral mucosae of the collected turbinates were separated from the underlying bone with surgical scissors. The turbinate mucosae and nasal polyps were then subjected to the following process.

Preparation of mucosal pieces for video recording

The turbinate and nasal polyp mucosae were cut into slender strips, including the mucosal surface along the long axis, using a razor blade. Two mucosal strips lying at right angles to each other were prepared from each sample. In the turbinate mucosae, the two strips were cut parallel to the horizontal and vertical axes, respectively. The mucosal strips were immediately immersed in O_2-saturated HBSS and transferred into a 20 x 6 x 1-mm test chamber filled with the same solution containing 0.05% (v/v) India ink as a tracer. Mucociliary beating/transport was observed under a Nikon Eclipse 80i phase-contrast light microscope (Nikon, Tokyo, Japan) equipped with a high-speed digital imaging system HAS-U1 (DITECT, Tokyo, Japan). Four recordings of 2-3 sec each were made at 60-sec intervals at a speed of 200 frames/sec and analyzed by HAS-XViewer Camera Memory ver. 1.2.12
(DITECT). All procedures were performed at room temperature (approx. 24^oC) and completed within 3 hrs after sample collection.

Measurement of mucociliary transport velocity (MCTV)

The MCTV of each mucosal strip was determined by measuring the distance traveled of India ink microparticles per unit time. The actual MCTV was calculated by the following formula:

$$\text{Actual MCTV} = \sqrt{\text{MCTV}_x{}^2 + \text{MCTV}_y{}^2}\ ,$$

where $MCTV_x$ and $MCTV_y$ are the MCTVs along the paired mucosal strips lying at right angles to each other. Then, the actual MCTVs of the right and left turbinates were averaged in each patient.

Measurement of ciliary beat frequency (CBF)

The number of ciliary beats was counted manually by checking the video in a slow replay mode. CBF was measured at three different sites of each mucosal strip. The CBF value in each patient was determined by averaging 16 measurements (4 recordings x 2 mucosal strips x both sides).

Fluorescence immunohistochemistry

The specimens were fixed with 4% paraformaldehyde in 0.1 M phosphate buffer at pH 7.4 (PB) at 4°C overnight. The fixed samples were transferred into a solution of 20% sucrose in 0.1 M phosphate-buffered saline at pH 7.4 (PBS) and incubated at 4^{o}C for 2 nights with 3-4 changes of solution. The samples were then frozen while embedded in Tissue-Tek OCT compound (Sakura Finetek, Tokyo, Japan) and stored at -80^{o}C until sectioning. Seven-mm-thick sections were prepared using a cryostat, mounted on silane-coated glass slides (Superfrost; Matsunami Glass Industries, Osaka, Japan), and air-dried. The sections were hydrated in PBS with 0.3% Triton X-100 (PBST) for 20 min and treated with 1.5% normal goat serum in PBST for 1 hr.

Next, the sections were incubated with rabbit anti-human Dishevelled-1 polyclonal antibody (PAJ540Hu01; Cloud-Clone, Houston, TX, USA), rabbit anti-human Dishevelled-3 polyclonal antibody (PAL453Hu01; Cloud-Clone), rabbit anti-human Frizzled3 polyclonal antibody (CSB-PA882067ESR2HU; Cusabio, Houston, Tx, USA), rabbit anti-human Frizzled6 polyclonal antibody (G260; Assay Biotech, Fremont, CA, USA), mouse anti-human Prickle1 monoclonal antibody (sc-393034; Santa Cruz Biotechnology, Dallas, TX, USA), rabbit anti-human Prickle2 polyclonal antibody (CSB-PA773783ESR1HU; Cusabio), mouse anti-human Vangl1 monoclonal antibody (sc-166844; Santa Cruz Biotechnology), or mouse anti-human Vangl2 monoclonal antibody (sc-515187; Santa Cruz Biotechnology) at 4°C overnight. The primary antibodies were used at dilutions of 1:50 in PBST containing 0.5% bovine serum albumin (BSA). As a negative control, the primary antibodies were omitted from the process. After a brief rinse with PBST, the sections were reacted at room temperature for 2 hrs with a secondary antibody, Alexa Fluor 488-conjugated goat anti-rabbit IgG (Invitrogen, Eugene, OR, USA) for Dishevelled-1, Dishevelled-3, Frizzled3, Frizzled6 and Prickle2 or Alexa Fluor 488-conjugated goat anti-mouse IgG (Invitrogen) for Prickle1, Vangl1 and Vangl2, diluted 1:1000 in PBST containing 0.5% BSA. The sections were coverslipped with Prolong Gold antifade reagent containing 4',6-diamidino-2-phenylindole dihydrochloride (DAPI; Invitrogen) and examined under a Carl Zeiss Axioskop 2 Plus fluorescence microscope. The light source was an HBO 103 W/2 mercury vapor lamp. The light passed through specific wavelength bandpass filters for excitation: 475-495 nm for Alexa Fluor 488 and 340-380 nm for

DAPI. Similarly, the emitted fluorescence passed through a 515-565 nm bandpass filter for Alexa Fluor 488 and a 435-485 nm bandpass filter for DAPI. Images were captured using a Carl Zeiss AxioCam digital camera attached to the microscope.

Preparation of total RNA

The collected tissues were minced with surgical scissors, soaked in 1 ml TRIzol Reagent (Invitrogen), and sonicated by an ultrasonic homogenizer (Taitec, Saitama, Japan). Two hundred ml chloroform was added, and after thorough shaking, the mixture was centrifuged at 22,000 xg for 15 min at 4^{o}C. The aqueous layer was transferred to another tube, and total RNA was extracted by the acid guanidiniumthiocyanate-phenol-chloroform method and cleaned up with a BioRobot EZ1 system (QIAGEN, Hilden, Germany), which enables fully automated extraction and purification of nucleic acids by magnetic bead technology. The purity of RNA was assessed by determining the ratio of light absorption at 260 nm (A_{260}) to that at 280 nm (A_{280}). An A_{260}/A_{280} ratio in the 1.9-2.1 range was considered acceptable. The RNA concentration was determined from A_{260}.

Quantitative reverse transcription-polymerase chain reaction (qRT-PCR)

The total RNA was reverse-transcribed to cDNA with a High-Capacity RNA-to-cDNA Kit (Applied Biosystems, Foster City, CA, USA), which uses random primers. The real-time RT-PCR analysis was performed with an Applied Biosystems StepOnePlus real-time PCR system using TaqMan Fast Universal PCR Master Mix (Applied Biosystems) with *glyceraldehyde-3-phosphate dehydrogenase* (*GAPDH*) as a housekeeping gene according to the manufacturer's instructions. The TaqMan Gene Expression Assays for *Dishevelled-1* (*DVL1*; assay identification number Hs00182896_m1), *Dishevelled-3* (*DVL3*; assay identification number Hs00610263_m1), *Frizzled3* (*FZD3*; assay identification number Hs00907280_m1), *Frizzled6* (*FZD6*; assay identification number Hs00171574_m1), *Prickle1* (*PRICKLE1*; assay identification number Hs01055551_m1), *Prickle2* (*PRICKLE2*; assay identification number Hs00291033_s1), *Vangl1* (*VANGL1*; assay identification number Hs01572998_m1), *Vangl2* (*VANGL2*; assay identification number Hs00393412_m1), and *GAPDH* (assay identification number Hs99999905_m1) were purchased from Applied Biosystems. Ten ng cDNA in 1 µl reaction buffer was mixed with TaqMan Universal PCR Master Mix with AmpErase (uracil N-glycosylase) and the primer/probe set of the TaqMan Gene Expression Assays, and the mixture was subjected to PCR amplification with real-time detection. The thermal cycler conditions were as follows: holding at 95^{o}C for 2 min, followed by 40 cycles of a two-step polymerase chain reaction of 95^{o}C for 1 sec and 60^{o}C for 20 sec. Each sample was assayed in duplicate. The measured threshold cycle (C_T) was normalized by subtracting the C_T for *GAPDH* of each sample from those for the target mRNAs. From the obtained DC_T values, the ratio of the target mRNA to *GAPDH* mRNA was calculated by the following formula:

Target mRNA/*GAPDH* mRNA ratio = $2^{-\Delta C}{}_T$.

Statistical analysis

Data are expressed as means ± SEM. Statistical analysis was performed with BellCurve for Excel Statistics (Social Survey Research Information Co., Tokyo, Japan). Differences between two groups were analyzed by the two-tailed Student *t*-test. *P*-values <0.05 were considered significant.

Results

The mean actual MCTV of nasal polyps was 7.43 ± 2.01 mm/s, which was significantly less than that of the turbinate mucosae (14.56 ± 2.09 mm/s, *P*=0.0361; Fig. 1). On the other hand, CBF was not statistically different between the two tissues (7.47 ± 0.13 Hz (turbinate) vs. 7.83 ± 0.23 Hz (nasal polyp), *P*=0.1699; Fig. 2), consistent with our previous observation [6]. Fig. 3 shows the MCTV vector of each turbinate. The vector was pointed toward the posteroinferior direction in all turbinates with an average inclination angle of 41.0 degrees.

Fig. 4 represents photomicrographs of fluorescence immunohistochemical staining of the turbinate mucosae and nasal polyp tissue for 8 different PCP proteins; Dishevelled-1, Dishevelled-3, Frizzled3, Frizzled6, Prickle1, Prickle2, Vangl1, and Vangl2. Moderate and weak fluorescence was observed for Dishevelled-1 and Dishevelled-3, respectively, on the surface of the turbinate mucosa, whereas the nasal polyps showed no immunoreactivity for these proteins (Figs. 4A and B). For Frizzled3, strong and weak fluorescence was seen on the surface of the turbinate mucosa and nasal polyp, respectively (Fig. 4C). Frizzled6 showed weak and moderate fluorescence on the surface and in the basal layer of the turbinate epithelium, respectively, but no immunoreactivity was detected in the nasal polyps. (Fig. 4D). For Prickle2, moderate and weak fluorescence was seen on the surface of the turbinate mucosa and nasal polyp, respectively (Fig. 4F). For Vangl2, weak fluorescence was observed on the surface of the turbinate mucosa, whereas the nasal polyp showed no immunoreactivity (Fig. 4H). No immunoreactivity was observed in either the turbinate mucosa or nasal polyp for Prickle1 or Vangl1 (Figs. 4E and G).

Fig. 5 shows the expression level of mRNA for each of the 8 PCP proteins, *DVL1*, *DVL3*, *FZD3*, *FZD6*, *PRICKLE1*, *PRICKLE2*, *VANGL1*, and *VANGL2*. The expression levels of *DVL1*, *DVL3* and *FZD3* mRNAs were significantly lower in the nasal polyps than in the turbinates (Figs. 5A-C), while those of *FZD6*, *PRICKLE1*, *PRICKLE2*, *VANGL1* and *VANGL2* mRNAs were not statistically different between the two tissues (Figs. 5D-H).

The results of immunohistochemistry and qRT-PCR are summarized in Table 1.

Table 1. Summary of immunohistochemistry and qRT-PCR

	Immunohistochemistry		qRT-PCR	
	Turbinate	Polyp	Turbinate	Polyp
Dishevelled-1	++	-	>	
Dishevelled-3	+	-	>	
Frizzled3	+++	+	>	
Frizzled6	++	-	≒	
Prickle1	-	-	≒	
Prickle2	++	+	≒	
Vangl1	-	-	≒	
Vangl2	+	-	≒	

-, +, ++ and +++ indicate no, weak, moderate and strong fluorescence, respectively.

Discussion

The present study showed that mucociliary transport is suppressed even though active mucociliary beating is maintained in nasal polyps compared to turbinate mucosae. Our study also revealed decreased immunohistochemical expressions of the PCP proteins, Dishevelled-1, Dishevelled-3, Frizzled3, Frizzled6, Prickle2 and Vangl2 in the nasal polyp compared to the turbinate mucosa. The expression levels of Dishevelled-1, Dishevelled-3 and Frizzled3 in the nasal polyps were also decreased at the transcriptional level.

Generally speaking, epithelial cells exhibit two-way polarity: polarity along the apical-basal axis and that across the plane of the epithelial sheet. The latter is referred to as PCP, an essential property for regulating epithelial tissue integrity and its developmental process [7]. The airway epithelial surface is lined with numerous ciliated cells. Each ciliated cell has 200 to 300 motile cilia on its apical surface [8]. The cilia are continuously beating to eliminate foreign bodies from the mucosal surface, an important frontline defense mechanism in this tissue. The ciliary beating must be coordinated temporally and spatially to exert effective mucociliary transport function. To generate this coordinated beating, the epithelial cells are arranged in an orderly fashion that makes use of a specific signaling pathway involving the PCP proteins.

Frizzled and Dishevelled are core PCP proteins that constitute the Wnt signaling pathway. There are three main Wnt pathways: the canonical b-catenin-dependent pathway, the noncanonical Wnt/calcium pathway, and the noncanonical Wnt/PCP pathway [7, 9]. The last pathway plays a critical role in PCP formation, and has been investigated in various organs and tissues, such as epithelial tissue [10], lung [9],

cochlea [11, 12], bile duct [13], kidney [14, 15], vasculature [16], neural tube/crest [11, 17-19], gastrula [17], and malignant tumors [20].

Frizzled is a four-span transmembrane protein acting as a Wnt receptor. Dishevelled is a cytoplasmic protein that binds to the intracellular domain of Frizzled. Ten isoforms of Frizzled (Frizzled1-10) and 3 isoforms of Dishevelled (Dishevelled-1, 2 and 3) have been identified in vertebrates. Previous researchers have explored the subcellular localization of these proteins in cultured airway epithelial cells and the *Drosophila* wing epithelium: Frizzled and Dishevelled are eccentrically localized on a specific side of the apical surface of the cells [21-23].

Vangl and Prickle are another pair of core PCP proteins: Vangl is a four-span transmembrane protein, and Prickle is a cytoplasmic protein that binds to the intracellular domain of Vangl [7, 9]. In vertebrates, each protein has two isoforms, Vangl1/2 and Prickle1/2. These molecules are also involved in the noncanonical Wnt/PCP pathway [24]. Like the Frizzled/Dishevelled complex, the Vangl/Prickle complex is eccentrically localized on the apical surface of the epithelial cells, but on the opposite side of Frizzled/Dishevelled [7, 9].

The present results clearly showed that the expression levels of Frizzled and Dishevelled are decreased in nasal polyps at the transcriptional and protein levels, implying the suppression of the Wnt signaling pathways, including the noncanonical Wnt/PCP pathway. The direction of ciliary beating is determined by the microtubule arrangement of the ciliary axoneme. Suppression of the noncanonical Wnt/PCP pathway in nasal polyps would lead to disarrangement of the direction of ciliary beating among ciliated epithelial cells, and consequently, inefficient mucociliary transport function despite the active ciliary beating of each cell. The present study also showed decreased immunohistochemical expression of Prickle2 and Vangl2 in nasal polyps, and this may also contribute to PCP disarrangement in this tissue.

In cultured epithelial cells, we can observe mucociliary beating and transport movement as a surface image taken from above [25]. If this method had been feasible for the excised tissue samples in the present study, we would have been able to directly determine the actual MCTV and the direction of the MCTV vector. However, the thickness of the tissue hindered the clear surface view required for obtaining such a surface image. To overcome this problem, two slender mucosal strips were cut at right angles to each other, and mucociliary beating and transport movement were observed from the side. Then, the actual MCTV and its direction were determined mathematically. The obtained *ex vivo* data in the present study are thought to reflect the *in vivo* phenomenon faithfully and are more valuable than those obtained from cultured cells.

Interestingly, the direction of mucociliary transport was pointed posteroinferiorly in all turbinate mucosa in the present study. Observations in previous *in vivo* human studies using tracers, such as saccharin, radioisotope, dye, and charcoal powder, have indicated that mucociliary transport on the medial surface of the inferior turbinate is directed to the posterior [26-29]. We examined the lateral surface mucosa of the turbinate in the present study and obtained a similar result. Through this mucociliary transport function, foreign particles on the turbinate mucosa are conveyed posteriorly, reach the pharynx, and then proceed

down the esophagus into the stomach, which is an efficient mechanism in the mucosal defense of the nose. Signaling pathways that determine the PCP direction, and thereby mucociliary transport direction, are of interest in connection with the frontline defense mechanism in the upper airway.

Conclusions

We investigated *ex vivo* mucociliary transport in nasal polyps and turbinate mucosae. The MCTV was significantly less in nasal polyps than in the turbinates despite the similar CBF of the two tissues. Immunohistochemical expressions of the PCP proteins, Dishevelled-1, Dishevelled-3, Frizzled3, Frizzled6, Prickle2 and Vangl2 were lower in the nasal polyps than in the turbinate mucosae. The expression levels of Dishevelled-1, Dishevelled-3 and Frizzled3 in the nasal polyps were also decreased at the transcriptional level. These results suggest that the decreased MCTV in the nasal polyps may be due to impaired PCP. Suppression of the Wnt pathway, which involves the PCP proteins, is likely to play a key role in the pathogenesis of the impaired mucociliary transport of nasal polyps. This point remains for further investigation.

Declarations

Author contributions: H.S. and T.K. planned and designed the study. T.N.N. and T.K. collected samples. T.N.N., Y.K. and H.S. measured the mucociliary transport velocity and ciliary beat frequency. T.N.N., Y.K. and T.W. performed immunohistochemistry and RT-PCR. T.N.N., Y.K., T.W. and T.K. analyzed data. T.N.N., Y.K. and H.S. wrote the manuscript.

Conflict of interest: The authors have no conflict of interests to declare.

Funding: This study was supported by a Grant-in-Aid for Scientific Research (C) (no. 19K09879; 2019-2022) to H.S. from the Japan Society for the Promotion of Science.

Ethics approval: Written informed consent was obtained from all the patients enrolled in the study. The study was approved by the institutional review board of the University of Occupational and Environmental Health (UOEHCRB19-014) and conducted in accordance with the World Medical Association Declaration of Helsinki. Two of the enrolled patients were under 20 years of age. In these patients, informed assent of the patients and informed consent of their parent(s) were obtained according to the protocol of the institutional review board.

References

1. Ikeda K, Oshima T, Furukawa M, Katori Y, Shimomura A, Takasaka T, Maruoka S (1997) Restoration of the mucociliary clearance of the maxillary sinus after endoscopic sinus surgery. J Allergy Clin Immunol 99: 48-52.
2. Asai K, Haruna S, Otori N, Yanagi K, Fukami M, Moriyama H (2000) Saccharin test of maxillary sinus mucociliary function after endoscopic sinus surgery. Laryngoscope 110: 117-122.

3. Sun SS, Hsieh JF, Tsai SC, Ho YJ, Kao CH (2002) Evaluation of nasal mucociliary clearance function in allergic rhinitis patients with technetium 99m-labeled macroaggregated albumin rhinoscintigraphy. Ann Otol Rhionl Laryngol 111: 77-79.
4. Sears PR, Bustamante-Marin XM, Gong H, Markovetz MR, Superfine R, Hill DB, Ostrowski LE 2021) Induction of ciliary orientation by matrix patterning and characterization of mucociliary transport. Biophys J 120: 1387-1395.
5. Yeh TH, Hsu WC, Chen YS, Hsu CJ, Lee SY (2005) Lipopolysaccharide decreases connexin 43 expression on nasal epithelial cells in vitro. Acta Otolaryngol 125: 1091-1096.
6. Do HB, Ohbuchi T, Yokoyama M, Kitamura T, Wakasugi T, Ohkubo J-I, Suzuki H (2019) Decreased ciliary beat responsiveness to acetylcholine in the nasal polyp epithelium. Clin Otolaryngol 44: 356-365.
7. Dreyer CA, VanderVorst K, Carraway KL 3rd (2022) Vangl as a master scaffold for Wnt/planar cell polarity signaling in development and disease. Front Cell Dev Biol 10: 887100.
8. Tilley AE, Walters MS, Shaykhiev R, Crystal RG (2015) Cilia dysfunction in lung disease. Annu Rev Physiol 77: 379-406.
9. Vlader EK, Konigshoff M (2020) Noncanonical Wnt planar cell polarity signaling in lung development and disease. Biochem Soc Trans 48: 231-243.
10. Yang Y, Mlodzik M (2015) Wnt-Frizzled/planar cell polarity signaling: cellular orientation by facing the wind (Wnt). Annu Rev Cell Dev Biol 31: 623-646.
11. Allache R, Lachance S, Guyot MC, De Marco P, Merello E, Justice MJ, Capra V, Kibar Z (2014) Novel mutations in Lrp6 orthologs in mouse and human neural tube defects affect a highly dosage-sensitive Wnt non-canonical planar cell polarity pathway. Hum Mol Genet 23: 1687-1699.
12. Landin Malt A, Clancy S, Hwang D, Liu A, Smith C, Smith M, Hatley M, Clemens C, Lu X (2021) Non-canonical Wnt signaling regulates cochlear outgrowth and planar cell polarity via Gsk3b inhibition. Front Cell Dev Biol 9: 649830.
13. Wilson DH, Jarman EJ, Mellin RP, Wilson ML, Waddell SH, Tsokkou P, Younger NT, Raven A, Bhalla SR, Noll AT, Olde Damink SW, Schaap FG, Chen P, Bates DO, Banales JM, Dean CH, Henderson DJ, Sansom OJ, Kendall TJ, Boulter L (2020) Non-canonical Wnt signalling regulates scarring in biliary disease via the planar cell polarity receptors. Nat Commun 11: 445.
14. Richards T, Modarage K, Dean C, McCarthy-Boxer A, Hilton H, Esapa C, Norman J, Wilson P, Goggolidou P (2019) Atmin modulates Pkhd1 expression and may mediate autosomal recessive polycystic kidney disease (ARPKD) through altered non-canonical Wnt/planar cell polarity (PCP) signalling. Biochim Biophys Acta Mol Basis Dis 1865: 378-390.
15. Krneta-Stankic V, Corkins ME, Paulucci-Holthauzen A, Kloc M, Gladden AB, Miller RK (2021) The Wnt/PCP formin Daam1 derives cell-cell adhesion during nephron development. Cell Rep 36: 109340.
16. Descamps B, Sewduth R, Ferreira Tojais N, Jaspard B, Reynaud A, Sohet F, Lacolley P, Allieres C, Lamaziere JM, Moreau C, Dufourcq P, Couffinhal T, Duplaa C (2012) Frizzled 4 regulates arterial network organization through noncanonical Wnt/planar cell polarity signaling. Circ Res 110: 47-58.

17. Jussila M, Ciruna B (2017) Zebrafish models of non-canonical Wnt/planar cell polarity signalling: fishing for valuable insight into vertebrate polarized cell behavior. Wiley Interdiscip Rev Dev Biol 6: e267.
18. Wang M, de Marco P, Capra V, Kibar Z (2019) Update on the role of the non-canonical Wnt/planar cell polarity pathway in neural tube defects. Cells 8: 1198.
19. Mayor R, Theveneau E (2014) The role of the non-canonical Wnt-planar cell polarity pathway in neural crest migration. Biochem J 457: 19-26.
20. VanderVorst K, Hatakeyama J, Berg A, Lee H, Carraway KL 3rd (2018) Cellular and molecular mechanisms underlying planar cell polarity pathway contributions to cancer malignancy. Semin Cell Dev Biol 81: 78-87.
21. Vladar EK, Bayly RD, Sangoram AM, Scott MP, Axelrod JD (2012) Microtubules enable the planar cell polarity of airway cells. Curr Biol 22: 2203-2212.
22. Strutt DI (2001) Asymmetric localization of Frizzled and the establishment of cell polarity in the *Drosophila* wing. Mol Cell 7: 367-375.
23. Axelrod JD (2001) Unipolar membrane association of Dishevelled mediates Frizzled planar cell polarity signaling. Genes Dev 15: 1182-1187.
24. Pataki CA, Couchman JR, Brabek J (2015) Wnt signaling cascades and the roles of syndecan proteoglycans. J Histochem Cytochem 63: 465-480.
25. Yasuda M, Inui T, Hirano S, Asano S, Okazaki T, Inui T, Marunaka Y, Nakahari T (2020) Intracellular Cl- regulation of ciliary beating in ciliated human nasal epithelial cells: frequency and distance of ciliary beating observed by high-speed video microscopy. Int J Mol Sci 21: 4052.
26. Kaya S, Ercan MT, Laleli Y (1984) Measurement of nasal mucociliary activity in man with ^{99m}Tc-labelled resin particles. Acta Otolaryngol 239: 267-272.
27. Passali D, Cappello C, Passali GC, Cingi C, Sarafoleanu C, Bellussi LM (2017) Nasal muco-ciliary transport time alteration: efficacy of 18b glycyrrhetinic acid. Multidiscip Respir Med 12: 29.
28. Paul B, Menon SS, Vasthare R, Balakrishnan R, Acharya S (2018) Effect of bidi smoking on nasal mucociliary clearance: a comparative study. J Laryngol Otol 2018; 132: 1077-1082.
29. Sahin E, Mamamci M, Kantekin Y (2020) Measurement of mucociliary clearance in the patients with multiple sclerosis. Eur Arch Otorhinolaryngol 277: 469-473.

Figures

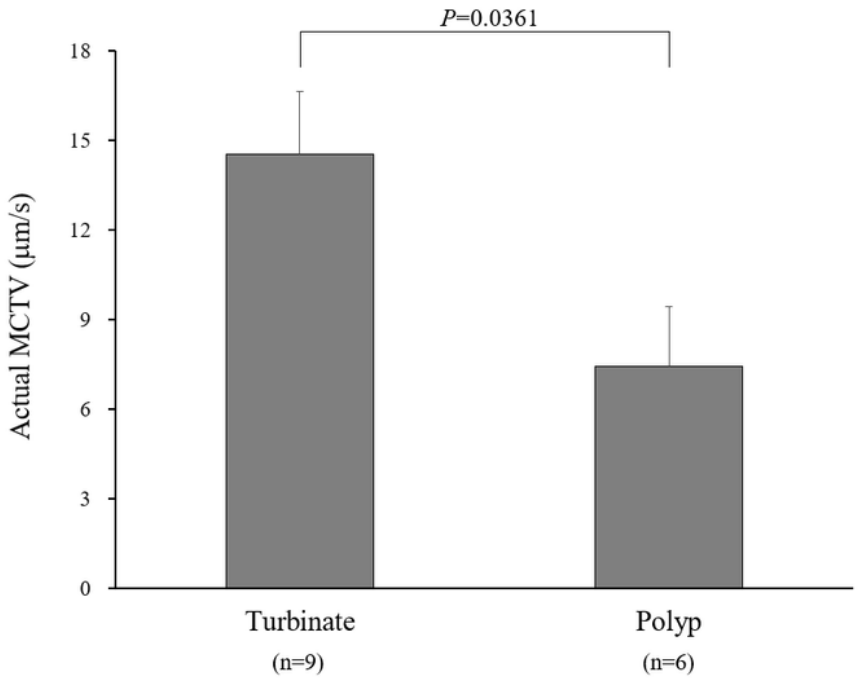

Figure 1

Fig. 1. MCTV of the turbinate and nasal polyp.

The turbinate and nasal polyp mucosae were cut into slender strips. Two mucosal strips lying at right angles to each other were prepared from each sample, immediately immersed in O_2-saturated HBSS and transferred into a test chamber filled with the same solution containing 0.05% (v/v) India ink as a tracer. Mucociliary transport was observed under a phase-contrast light microscope equipped with a high-speed digital video camera. The MCTV of each mucosal strip was determined by measuring the distance traveled of microparticles of India ink per unit time. The actual MCTV was calculated by the following formula:

Actual MCTV = $\sqrt{MCTV_x{}^2 + MCTV_y{}^2}$, where $MCTV_x$ and $MCTV_y$ are MCTVs along the paired mucosal strips lying at right angles to each other. Then, the actual MCTVs of the right and left turbinates were averaged for each patient.

MCTV, mucociliary transport velocity

HBSS, Hank's balanced salt solution

Figure 1

See image above for figure legend

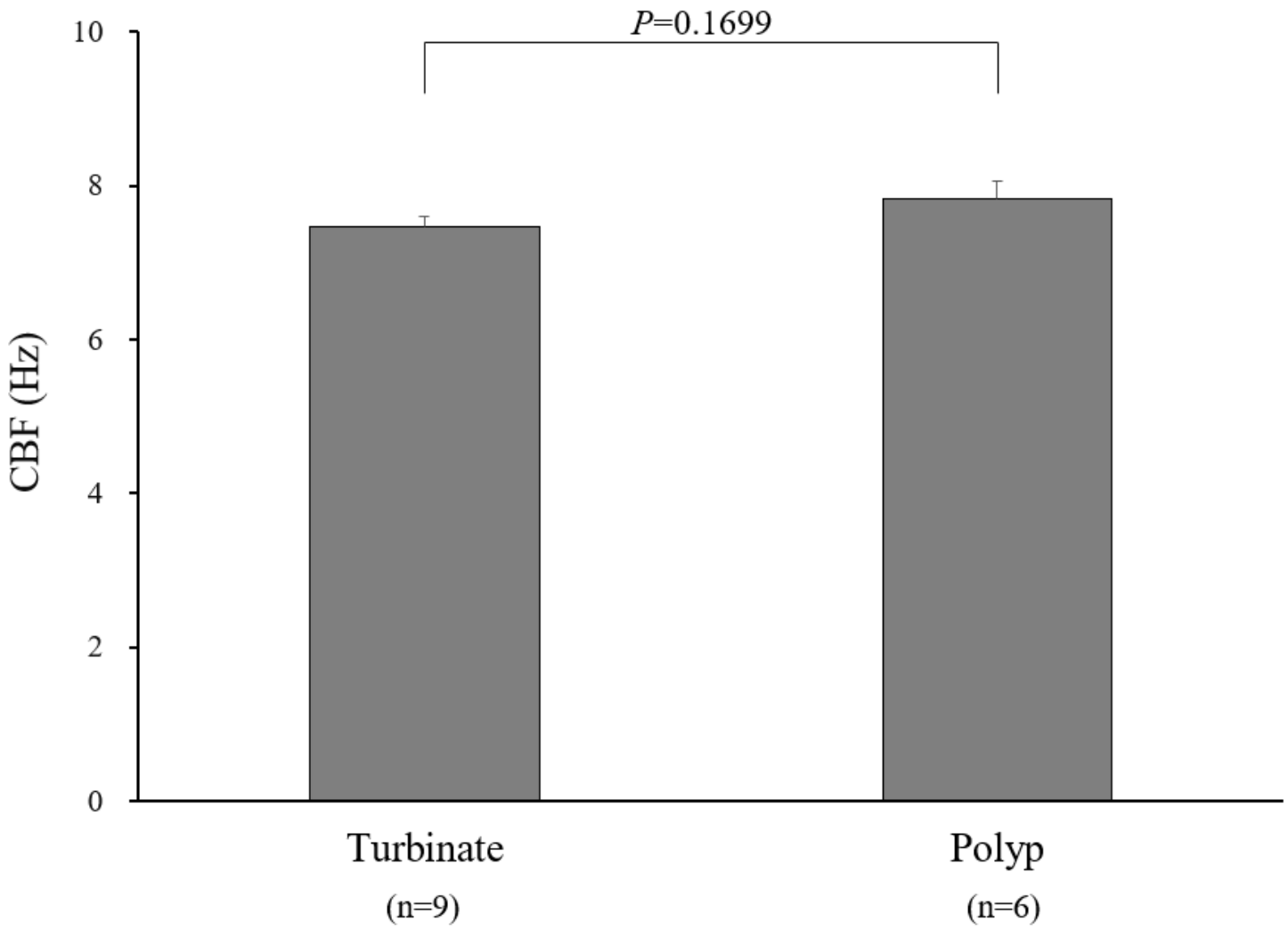

Figure 2

Figure 2

HBSS, Hank's balanced salt solution

CBF of the turbinate and nasal polyp.

The turbinate and nasal polyp mucosae were cut into slender strips, immediately immersed in O_2-saturated HBSS and transferred into a test chamber. Mucociliary beating was observed under a phase-contrast light microscope equipped with a high-speed digital imaging system. The number of ciliary beats was counted manually by checking the video in a slow replay mode.

CBF, ciliary beat frequency

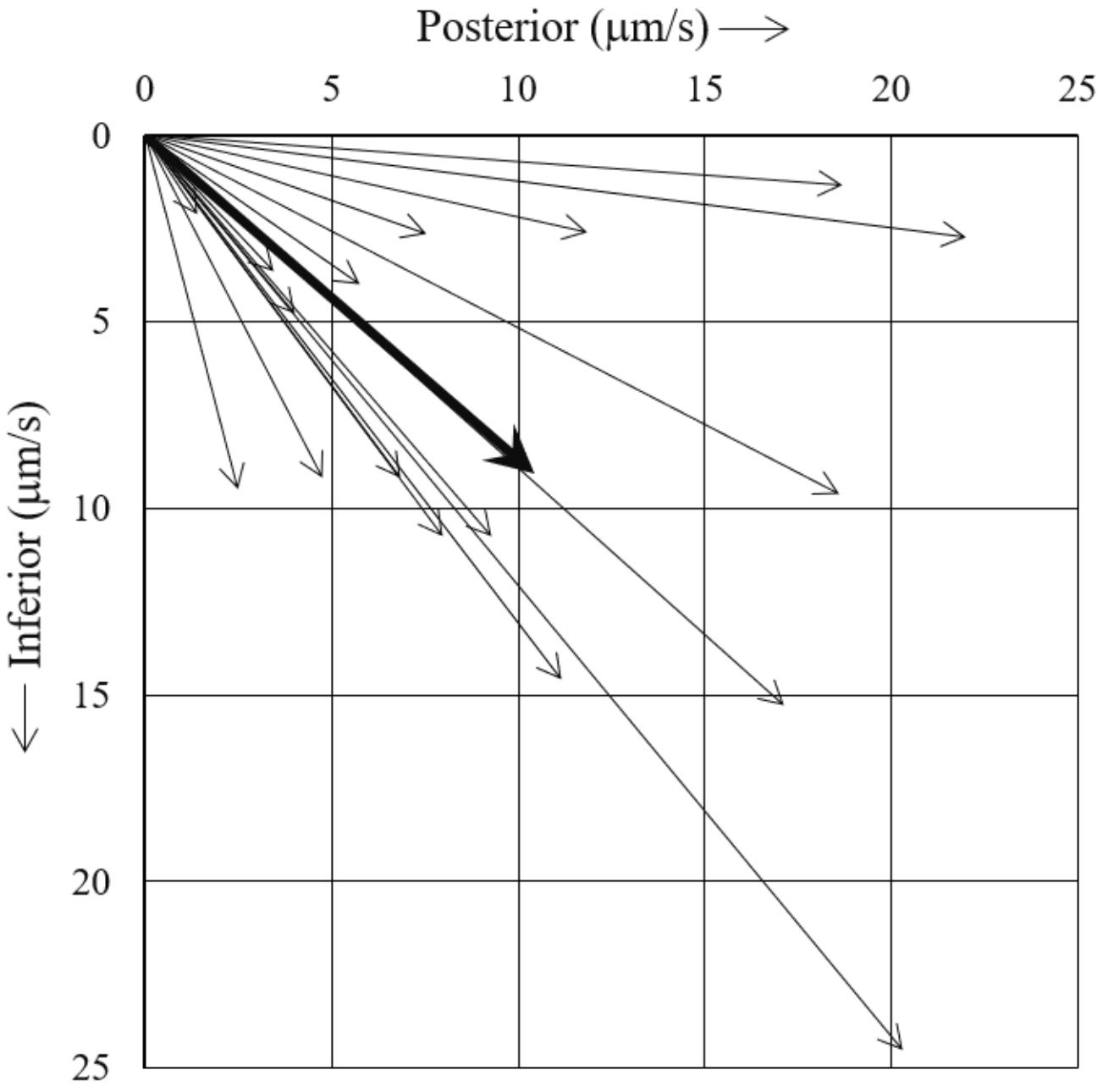

Figure 3

Figure 3

MCTV vector of each turbinate.

The MCTV vector pointed to the posteroinferior direction in all turbinates (thin arrows). The average inclination angle was 41.0 degrees (thick arrow).

MCTV; mucociliary transport velocity

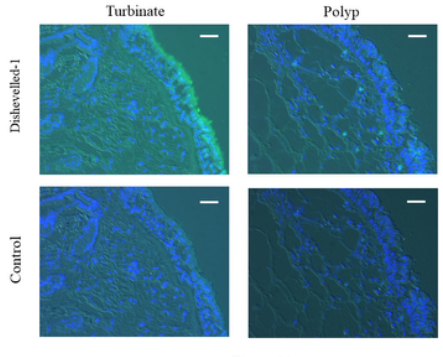

Figure 4A

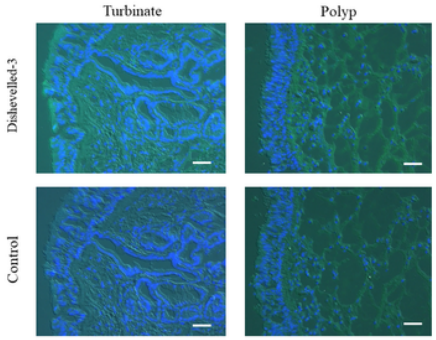

Figure 4B

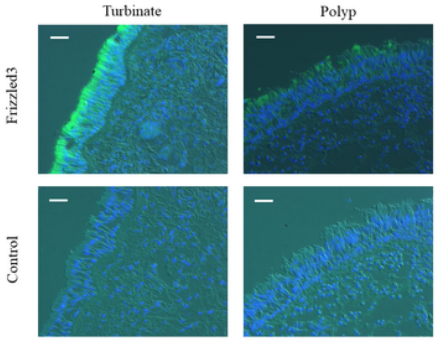

Figure 4C

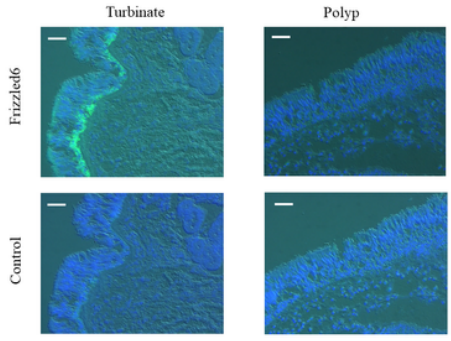

Figure 4D

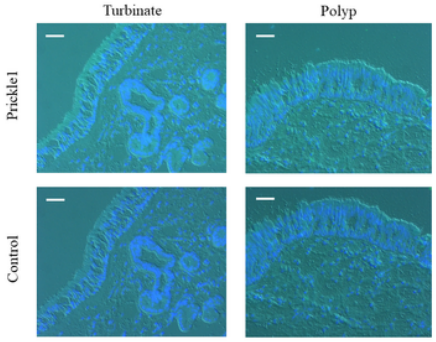

Figure 4E

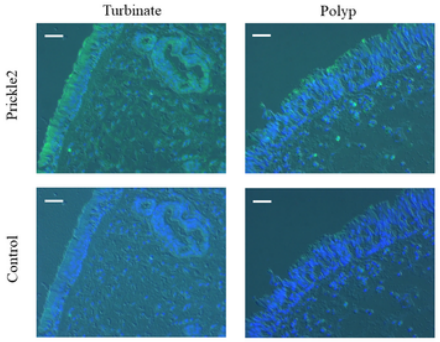

Figure 4F

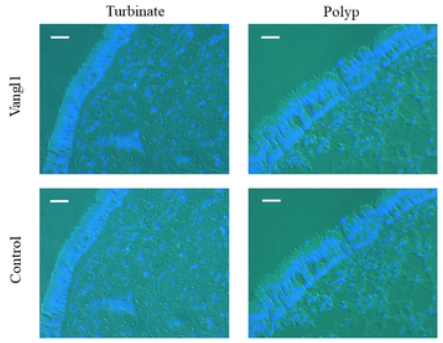

Figure 4G

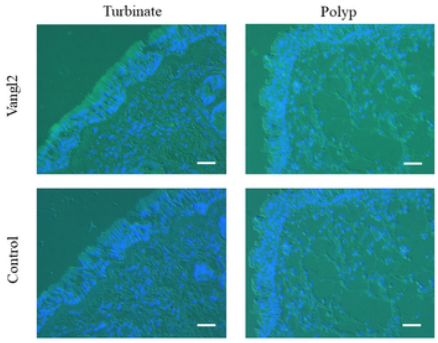

Figure 4H

Figure 4

Photomicrographs of fluorescence immunohistochemical staining of the turbinate and nasal polyp for the PCP proteins.

The turbinates and nasal polyps were fixed with 4% paraformaldehyde and embedded while frozen in Tissue-Tek OCT Compound. Seven-micrometer-thick sections were prepared, mounted on silane-coated glass slides, and incubated with a primary antibody. As a negative control, the primary antibody was omitted from the process. The sections were then reacted with a secondary antibody, Alexa Fluor 488-conjugated goat anti-rabbit or mouse IgG, coverslipped with Prolong Gold antifade reagent containing DAPI, and examined under a Carl Zeiss Axioskop 2 Plus fluorescence microscope. Images were captured

using a Carl Zeiss AxioCam digital camera attached to the microscope. Green and blue colors express the fluorescence of Alexa Fluor 488 and DAPI, respectively. Scale bar = 20 mm.

(A) Dishevelled-1. Moderate fluorescence is observed on the surface of the turbinate mucosa, whereas the nasal polyp shows no immunoreactivity.

(B) Dishevelled-3. Weak fluorescence is observed on the surface of the turbinate mucosa, whereas the nasal polyp shows no immunoreactivity.

(C) Frizzled3. Strong and weak fluorescence are seen on the surface of the turbinate mucosa and nasal polyp, respectively.

(D) Frizzled6. Weak and moderate fluorescence are observed on the surface and in the basal layer of the turbinate epithelium, respectively, while the nasal polyp shows no immunoreactivity.

(E) Prickle1. There is no immunoreactivity in either the turbinate mucosa or nasal polyp.

(F) Prickle2. Moderate and weak fluorescence are seen on the surface of the turbinate mucosa and nasal polyp, respectively.

(G) Vangl1. There is no immunoreactivity in either the turbinate mucosa or nasal polyp.

(H) Vangl2. Weak fluorescence is observed on the surface of the turbinate mucosa, whereas the nasal polyp shows no immunoreactivity.

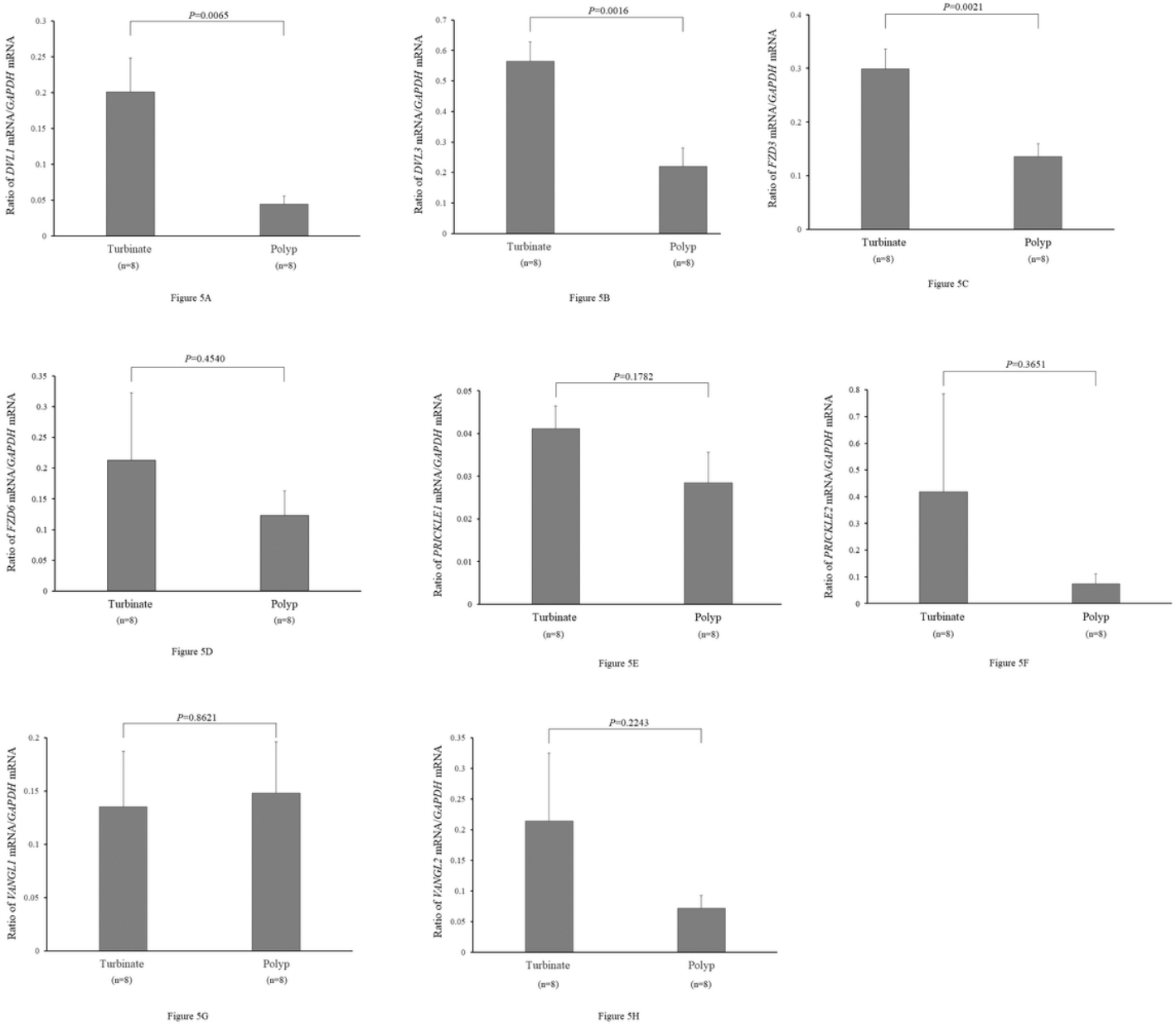

Figure 5

Expression levels of mRNAs for the PCP proteins in the turbinate and nasal polyp.

The turbinates and nasal polyps were minced and soaked in TRIzol reagent. Total RNA was extracted by the acid guanidiniumthiocyanate-phenol-chloroform method, cleaned up with a BioRobot EZ1 system, and reverse-transcribed to cDNA using a High-Capacity RNA-to-cDNA Kit. Quantitative reverse transcription-polymerase chain reaction analysis (PCR) was performed with an Applied Biosystems StepOnePlus real-time PCR system using TaqMan Fast Universal PCR Master Mix with glyceraldehyde-3-phosphate dehydrogenase (GAPDH) as a housekeeping gene. The thermal cycler conditions were as follows: holding at 95°C for 2 min, followed by two-step polymerase chain reaction of 40 cycles of 95°C for 1 s and 60°C for 20 s. The measured threshold cycle (C_T) was normalized by subtracting the

C_T for *GAPDH* of each sample from those for the target mRNAs. From the obtained ΔC_T values, the ratio of the target mRNA to *GAPDH* mRNA was calculated by the following formula:

Target mRNA/*GAPDH* mRNA ratio = $2^{-\Delta C}{}_T$.

(A) *DVL1*, (B) *DVL3*, (C) *FZD3*, (D) *FZD6*, (E) *PRICKLE1*, (F) *PRICKLE2*, (G) *VANGL1*,

(H) *VANGL2*.